SUPPLEMENTARY INFORMATION

Unique structured microspheres with multishells comprising graphitic carbon-coated Fe_3O_4 hollow nanopowders as anode materials for high-performance Li-ion batteries

Gi Dae Park[a], Jeong Hoo Hong[a], Dae Soo Jung[b] Jong-Heun Lee[a], and Yun Chan Kang*[a]

[a]*Department of Materials Science and Engineering, Korea University, Anam-Dong, Seongbuk-Gu, Seoul 136-713, Republic of Korea, E-mail: yckang@korea.ac.kr; Fax: (+82) 2-928-3584*

[b]*Energy and Environmental Division, Korea Institute of Ceramic Engineering and Technology, Jinju 660-031, Republic of Korea.*

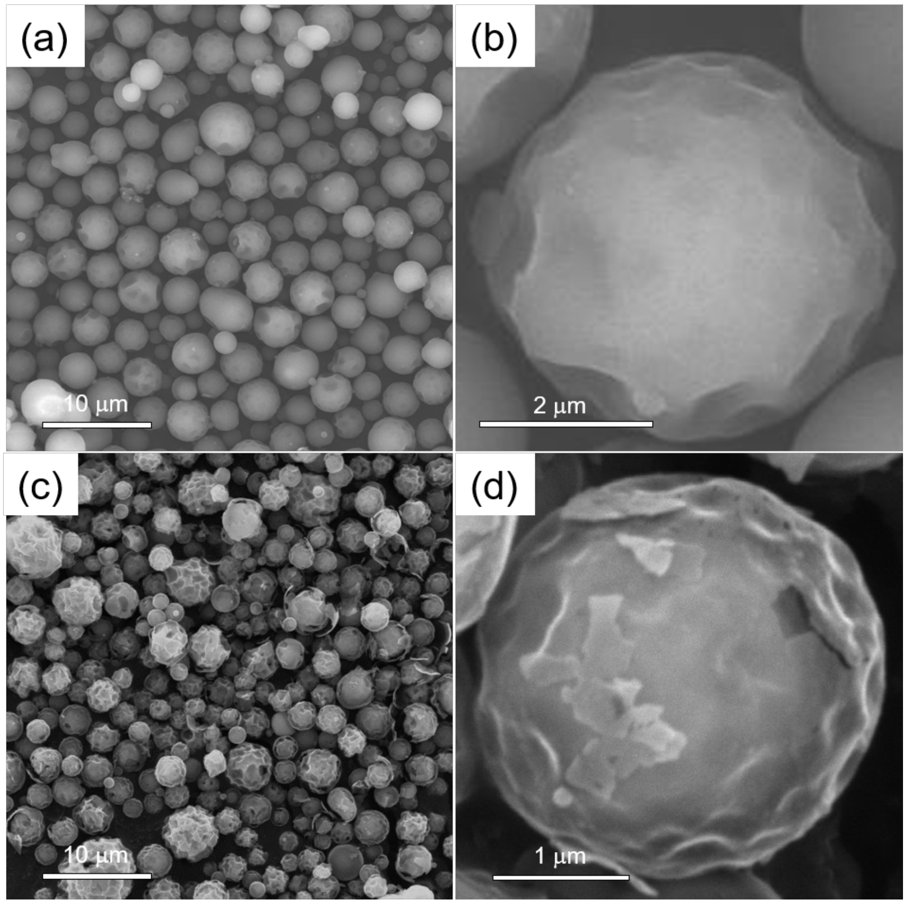

Fig. S1 Morphologies of microspheres synthesized by spray drying process before and after post-treatment process. (a,b) as-prepared and (c,d) post-treated microspheres.

.

.

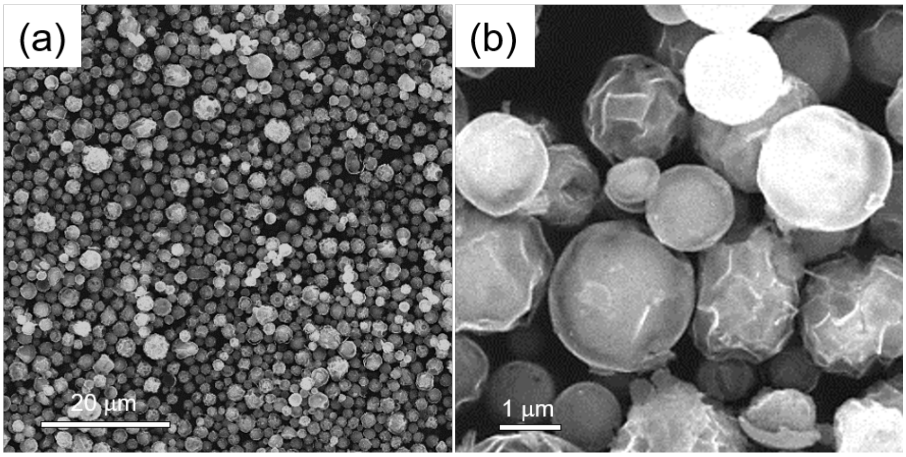

Fig. S2 Morphologies of pitch infiltrated Fe_2O_3 yolk-shell microspheres.

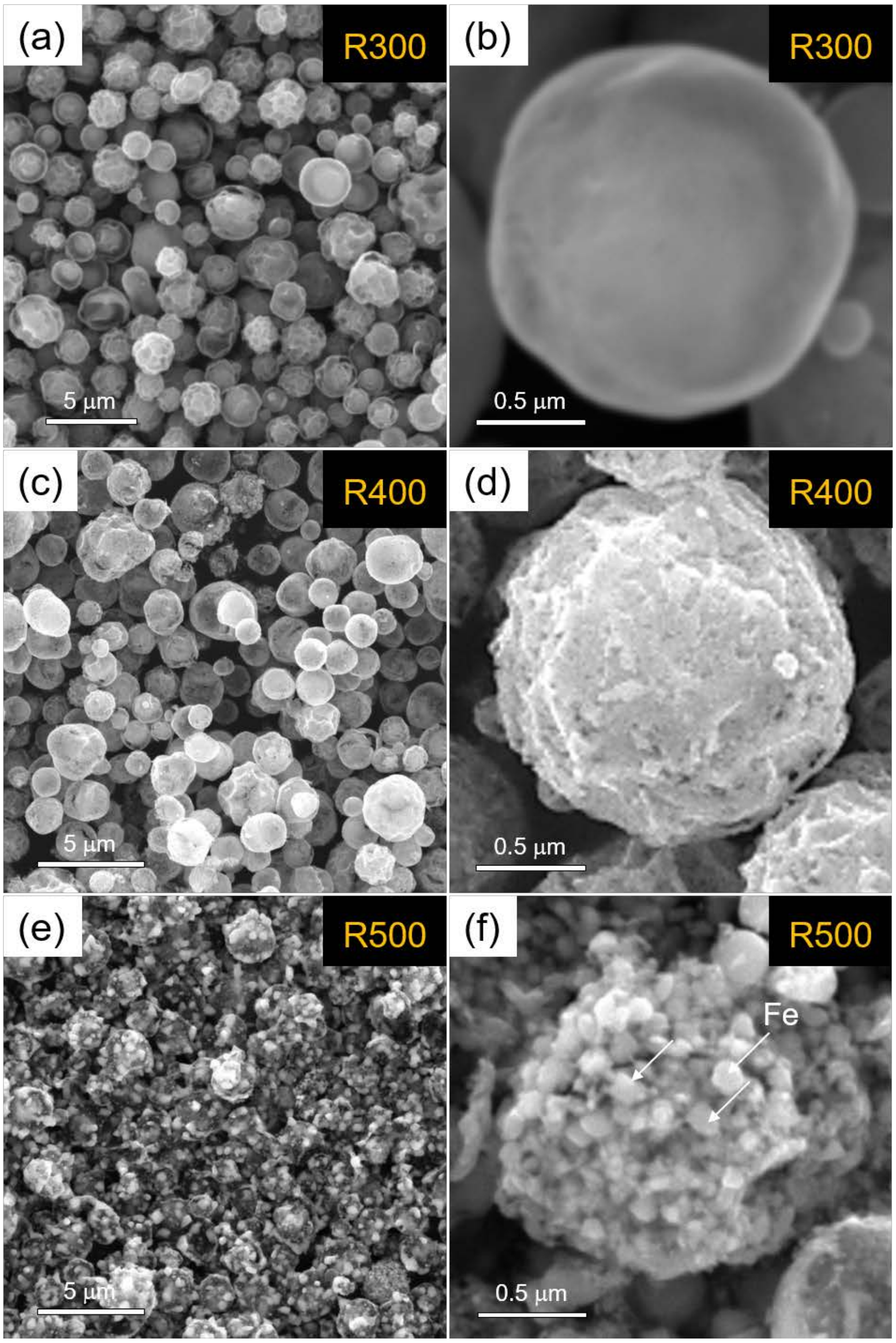

Fig. S3 Morphologies of microspheres formed after reduction process of pitch-infiltrated Fe_2O_3 yolk-shell microspheres at (a,b) 300 °C, (c,d) 400 °C, and (e,f) 500 °C.

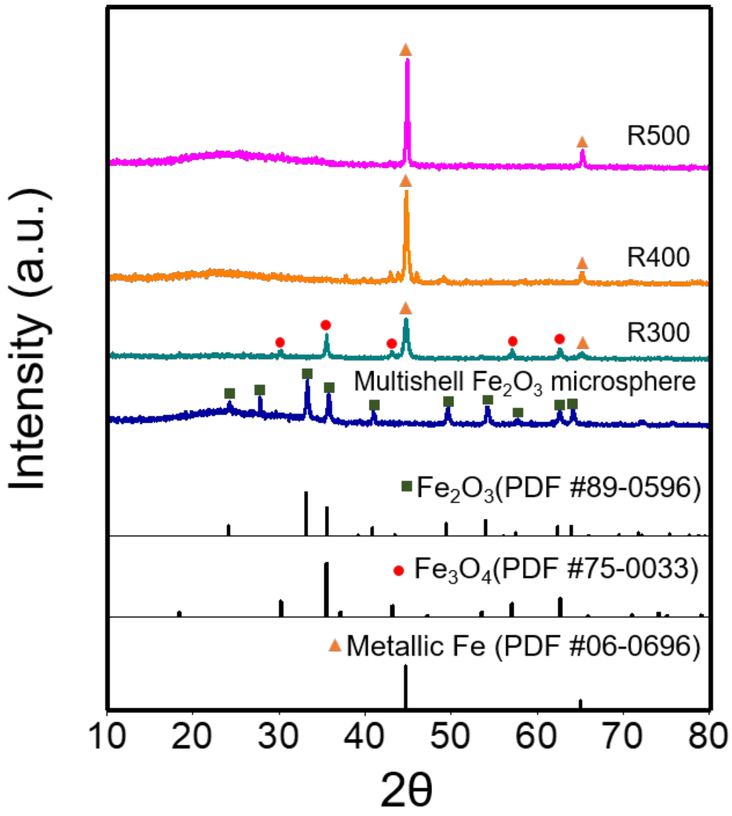

Fig. S4 XRD patterns of microspheres obtained before and after reduction process at 300 (R300), 400 (R400) and 500 °C (R500).

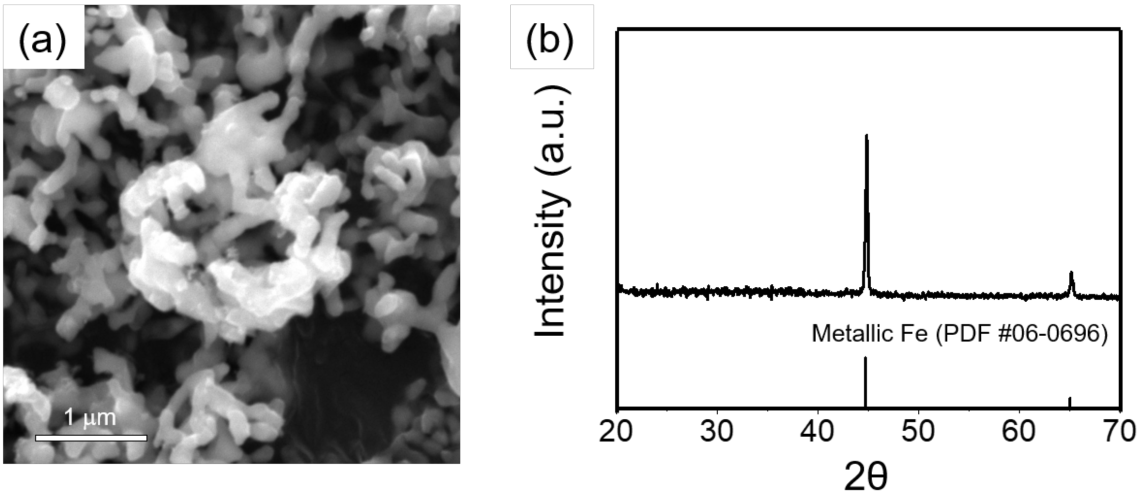

Fig. S5 (a) Morphology and (b) XRD pattern of metallic Fe powders formed after reduction of Fe_2O_3 yolk-shell microspheres at 400 °C.

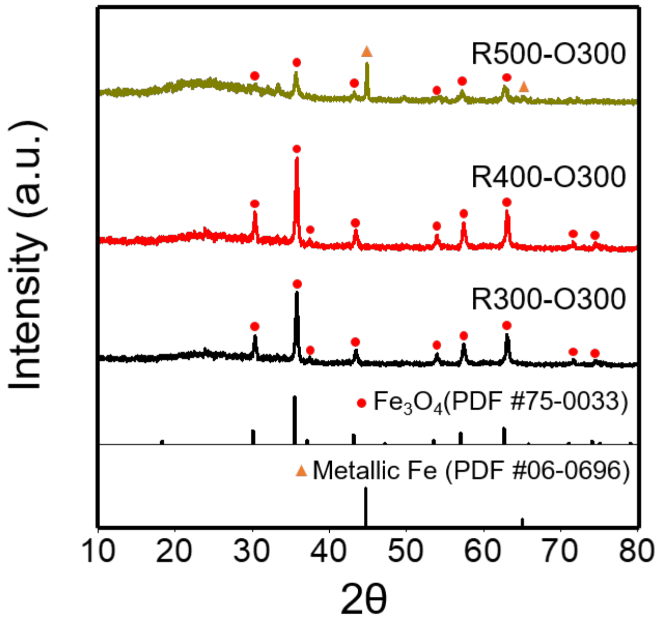

Fig. S6 XRD patterns of R300-O300, R400-O300, and R500-O300 microspheres.

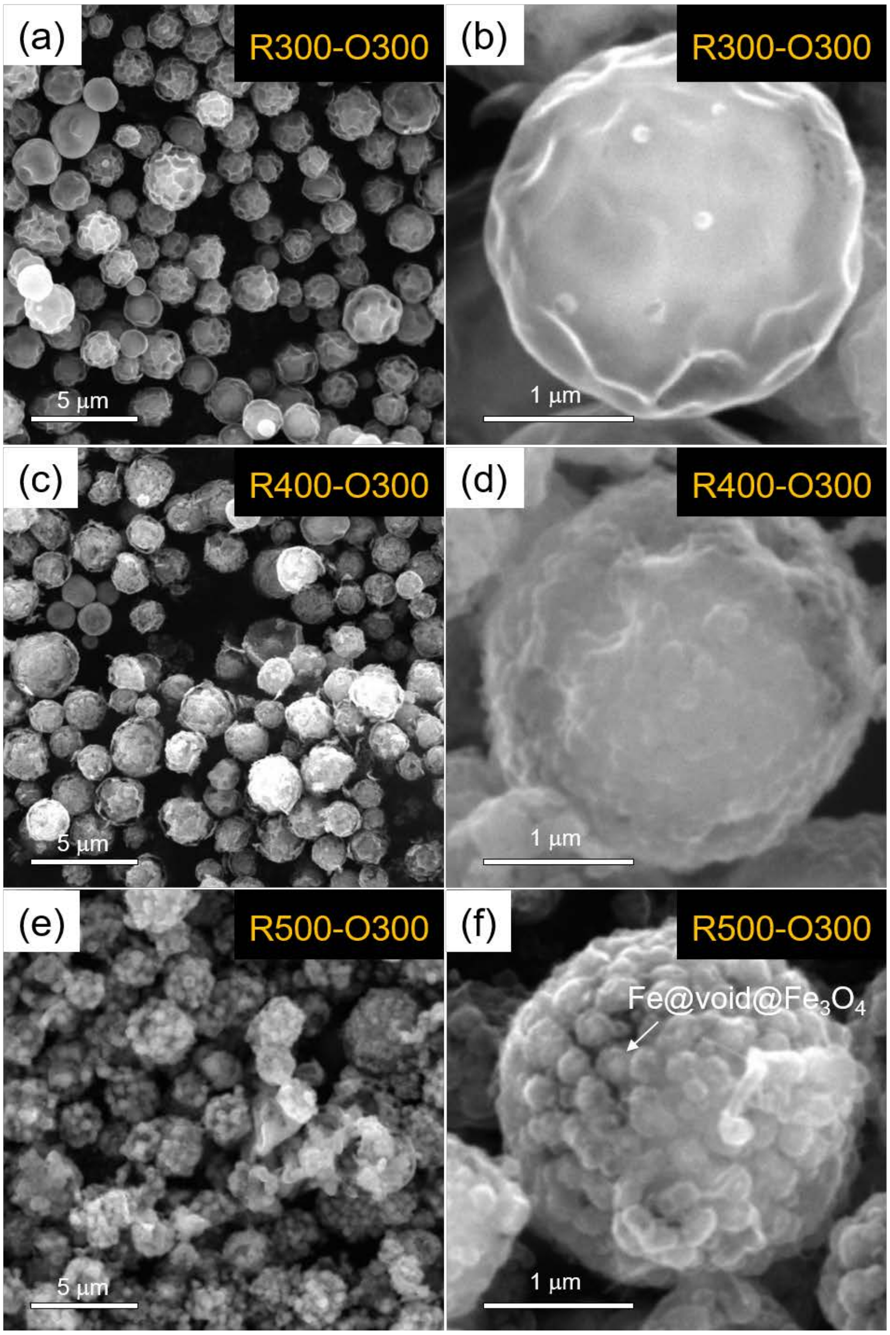

Fig. S7 Morphologies of (a,b) R300-O300, (c,d) R400-O300, and (e,f) R500-O300 microspheres.

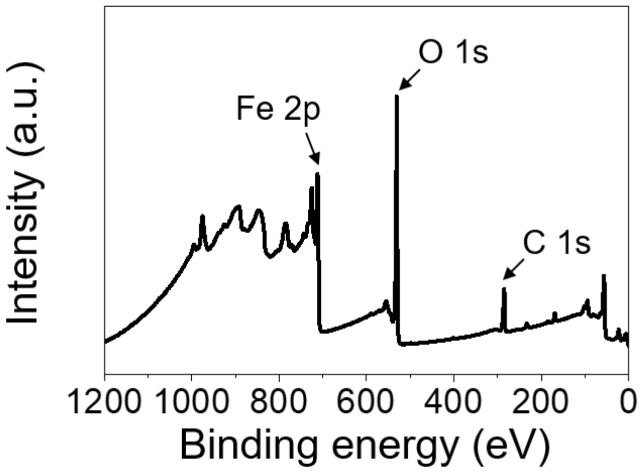

Fig. S8 XPS survey scan of Fe_3O_4-GC (R400-O300) microspheres.

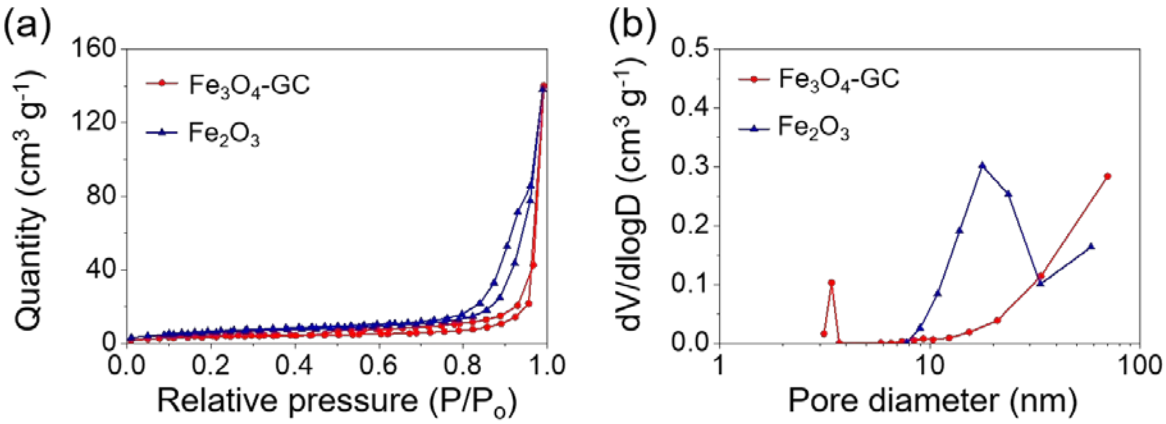

Fig. S9 (a) N_2 gas adsorption and desorption isotherm and (b) BJH pore-size distribution of Fe_3O_4-GC (R400-O300) and bare Fe_2O_3 microspheres.

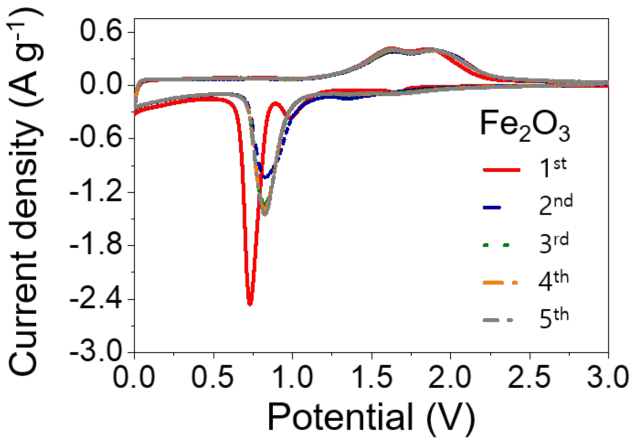

Fig. S10 CV curves of yolk-shell structured Fe_2O_3 microspheres.

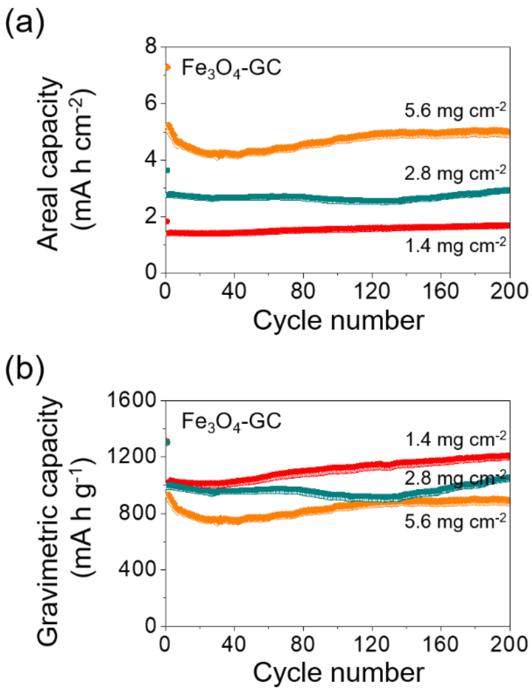

Fig. S11. (a) Areal and (b) gravimetric capacities of yolk-shell structured Fe_3O_4-GC composite microspheres at the different active materials mass loadings on the electrode.

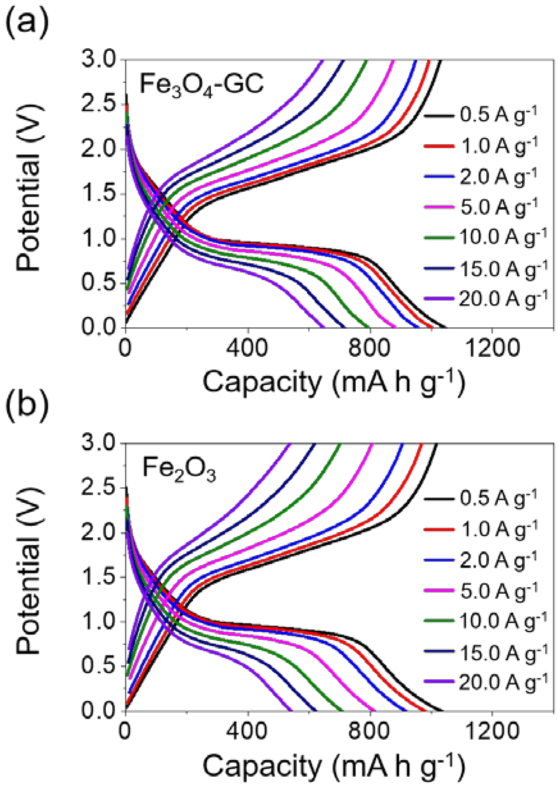

Fig. S12. Charge-discharge curves at different rates (0.5, 1, 2, 5, 10, 15, and 20 A g^{-1}) of yolk-shell structured Fe_3O_4-GC composite and Fe_2O_3 microspheres.

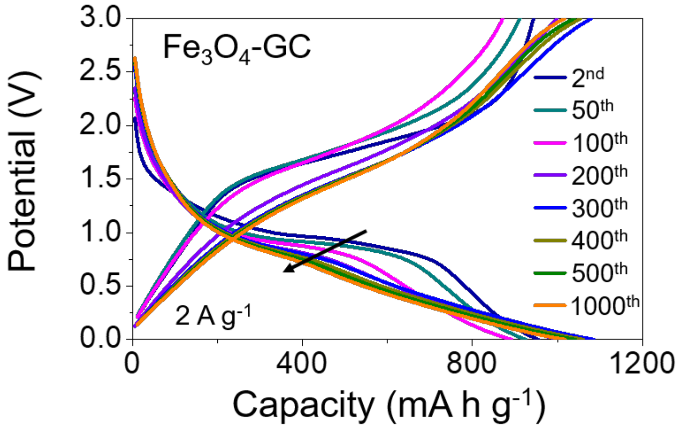

Fig. S13. The 2nd, 50th, 100th, 200th, 300th, 400th, 500th, and 1000th charge-discharge curves obtained during the long-term cycling test of yolk-shell structured Fe_3O_4-GC composite microspheres.

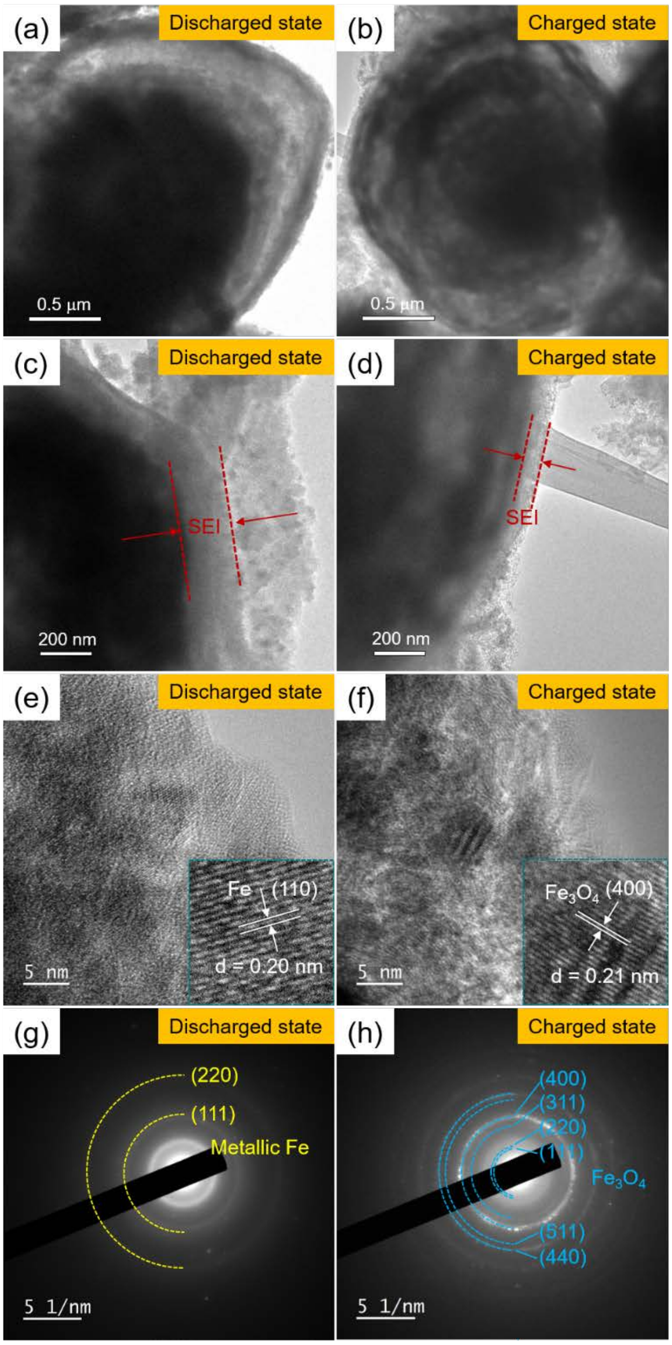

Fig. S14. TEM images and SAED patterns of yolk-shell strucutred Fe_3O_4-GC composite at fully (a,c,e,g) discharged and (b,d,f,h) charged states after 100 cycles : (a-d) TEM images, (e,f) HR-TEM images, (g,h) SAED pattern.

Table S1. Electrochemical properties of various Fe_3O_4 materials applied as lithium-ion batteries reported in the previous literatures.

Materials	Current rate	Discharge capacity [mA h g^{-1}] and (cycle number)	Rate capacity [mA h g^{-1}] (current rate)	Ref
Graphene-wrapped Fe_3O_4	0.7 A g^{-1}	~600 (100)	~600 (1.75 A g^{-1})	[S1]
Carbon coated Fe_3O_4 nanospindles	0.4 A g^{-1}	530 (80)	190 (4.0 A g^{-1})	[S2]
Carbon-encapsulated Fe_3O_4 nanoparticles	5.0 A g^{-1}	836 (350)	297 (20.0 A g^{-1})	[S3]
Dual layers N-doped carbon@ mesoporous carbon@Fe_3O_4 nanoparticle	2.0 A g^{-1}	576 (500)	322 (5.0 A g^{-1})	[S4]
Fe_3O_4-embedded and N-doped hierarchically porous carbon nanospheres	1.0 A g^{-1}	581 (400)	290 (10.0 A g^{-1})	[S5]
N-doped dual carbon-confined 3D architecture rGO/Fe_3O_4/AC	5.0 A g^{-1}	~500 (500)	437 (10.0 A g^{-1})	[S6]
Porous Fe_3O_4/carbon microspheres	1.0 A g^{-1}	746 (300)	410 (5.0 A g^{-1})	[S7]
Pomegranate-like, carbon-coated Fe_3O_4	5.0 A g^{-1}	520 (1000)	416 (10.0 A g^{-1})	[S8]
Neuron-inspired Fe_3O_4-conductive carbon	1.0 A g^{-1}	971 (1000)	206 (8.0 A g^{-1})	[S9]
Macroporous Fe_3O_4@C	2.0 A g^{-1}	645 (1000)	300 (10.0 A g^{-1})	[S10]
Yolk–shell-structured microsphere with multishells of hollow Fe_3O_4 nanopowders covered with GC	**2.0 A g^{-1}**	**1018 (1000)**	**649 (20.0 A g^{-1})**	**Our work**

References

[S1] G. Zhou, D.-W. Wang, F. Li, L. Zhang, N. Li, Z.-S. Wu, L. Wen, G. Q. Lu, H.-M. Cheng, *Chem. Mater.*, 2010, **22**, 5306-5313.

[S2] W.-M. Zhang, X.-L. Wu, J.-S. Hu, Y.-G. Guo, L.-J. Wan, *Adv. Funct. Mater.*, 2008, **18**, 3941-3946.

[S3] C. He, S. Wu, N. Zhao, C. Shi, E. Liu, J. Li, *ACS Nano*, 2013, **7**, 4459-4469.

[S4] B. Zhu, G. Guo, G. Wu, Y. Zhang, A. Dong, J. Hu, D. Yang, *J. Alloys Compd.*, 2019, **775**, 776-783.

[S5] J. Mao, D. Niu, N. Zheng, G. Jiang, W. Zhao, J. Shi, Y. Li, *ACS Sustainable Chem. Eng.*, 2019, **32**, 3424-3433.

[S6] R. Ding, J. Zhang, J. Qi, Z. Li, C. Wang, M. Chen, *ACS Appl. Mater. Interfaces*, 2018, **10**, 13470-13478.

[S7] W. Han, X. Qin, J. Wu, Q. Li, M. Liu, Y. Xia, H. Du, B. Li, F. Kang, *Nano Res.*, 2018, **11**, 892-904.

[S8] D. Han, G. Guo, Y. Yan, T. Li, B. Wang, A. Dong, *Energy Storage Mater.*, 2018, **10**, 32-39.

[S9] S.-M. Hao, Q.-J. Li, J. Qu, F. An, Y.-J. Zhang, Z.-Z. Yu, *ACS Appl. Mater. Interfaces*, 2018, **10**, 17923-17932.

[S10] Z. Yan, X. Jiang, Y. Dai, W. Xiao, X. Li, N. Du, G. He, *ACS Appl. Mater. Interfaces*, 2018, **10**, 2581-2590.